Double frustration and magnetoelectroelastic excitations in collinear multiferroic materials

D. C. Cabra

IFLySiB-CONICET-UNLP and Departamento de Física, Universidad Nacional de La Plata, 1900 La Plata, Argentina

A. O. Dobry ® and C. J. Gazza ®

*IFIR-CONICET-UNR and Facultad de Ciencias Exactas, Ingeniería y Agrimensura,
Universidad Nacional de Rosario, 2000 Rosario, Argentina*

G. L. Rossini ®

IFLP-CONICET-UNLP and Departamento de Física, Universidad Nacional de La Plata, 1900 La Plata, Argentina

We discuss a model scenario for multiferroic systems of type II (collinear spins) where the electric dipolar order competes with a frustrated magnetic order in determining the elastic distortions of the lattice ion positions. High magnetic frustration due to second-neighbors exchange and small spin easy-axis anisotropy lead to the appearance of the so-called quantum magnetic plateau states. Increasing the magnetic field above the plateau border produces composite excitations, where fractionalized spin tertions arise together with spontaneous dipolar flips (in the form of domain walls) and enhanced localized elastic distortions. This peculiar magnetoelectric effect may be described by magneto-electric-elastic quasiparticles that could be detected by x-ray and neutron diffraction techniques. Our results are supported by extensive DMRG computations on the spin sector and self-consistent equations for the lattice distortions.

I. INTRODUCTION

Multiferroic materials, in which magnetic and dipolar order coexist and interact, are currently under intense investigation. Elastic distortions of ionic positions, in the form of structural transitions, are deeply connected with the onset of magnetic and/or ferroelectric order. Some of these materials do not show signs of spin-orbit correlations, instead they exhibit collinear spin order and electric polarization below a common transition temperature; they are called improper type-II collinear multiferroics [1–3]. Several materials with such transitions are described in Refs. [4–14].

We have recently proposed a microscopic model in Ref. [15] describing the interaction between spins and electric dipoles in a quasi-one-dimensional multiferroic system via elastic distortions. A key ingredient of this model, shown in Fig. 1, is the variation of dipolar moments according to the distance between neighboring spin sites; as dipoles are shortened when spin separation is increased, the model reminds a pantograph mechanism. Thus the dipole-dipole interaction produces a back reaction of the dipolar degrees of freedom on the elastic distortions, and consequently in the magnetic sector. A salient feature is the observation of an ordered dipolar phase with period three, which shows up in the presence of an appropriate homogeneous external electric field (see Fig. 3 in Ref. [15]) because of the long-range character of dipolar interactions (cf. Ref. [16], where only nearest-neighbor (NN) dipolar interactions are discussed). Some properties of this dipolar phase, denoted as $\Uparrow\Uparrow\Downarrow$ in the following [17], motivate the present paper.

We investigate here the commensurability interplay of the $P = 1/3$ period-three dipolar order $\Uparrow\Uparrow\Downarrow$ [see Fig. 2(c) below] with the period-three magnetic configurations observed in many frustrated magnetic materials with $M = 1/3$ magnetization plateaus (M expressed as a fraction of saturation). In most studies, the $M = 1/3$ plateau state is found to form a collinear $\uparrow\uparrow\downarrow$ [see Fig. 2(b)] classical pattern [18], but a quantum $\bullet\!-\!\bullet \uparrow$ order [where $\bullet\!-\!\bullet$ stands for a spin singlet, see Fig. 2(a)] has been also predicted for spin $S = 1/2$ modulated isotropic Heisenberg chains [19]. The robustness of magnetic plateau states, given by an energy gap in the magnetization spectrum, makes them good candidates for technological applications. Relatedly, the characteristics of the elementary $\Delta S^z = 1$ excitations at the high field border of the plateaus deserve detailed analysis.

We find that the dipolar order introduced by the long-range dipolar interactions indeed competes with the magnetic order set by the magnetic frustration at the $M = 1/3$ plateau, opening a nontrivial scenario which we dub *double frustration*. Our analysis predicts unusual effects due to this scenario. For low anisotropy and high magnetic frustration, favoring quantum fluctuations, the double frustration stabilizes a quantum structure at the $M = 1/3$ plateau state. In contrast, either for higher easy-axis anisotropy or for lower magnetic frustration, or both, the double frustration competition leads to the spontaneous parity symmetry breaking of the classical collinear $M = 1/3$ plateau state. We must stress that, in a more general situation with charge order along the chain, parity breaking would imply the appearance of longitudinal electric polarization [2]. These results are clear signals of the role of dipolar
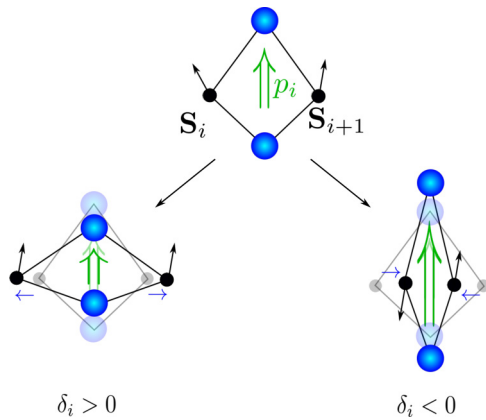
FIG. 1. Schematic picture for the pantograph mechanism coupling electric dipoles to the lattice. Black dots represent magnetic sites and blue spheres represent a charge distribution, giving rise to dipolar moments. Green double arrows represent these dipolar moments that might point up or down. Displacements of magnetic sites, indicated by blue arrows, produce lattice bond length distortions δ_i that modify the strength of local dipoles.

interactions and may guide the search for materials realizing strong magnetoelectric effects.

After analyzing the plateau states, we discuss the excitations caused by the increase of the magnetic field. We
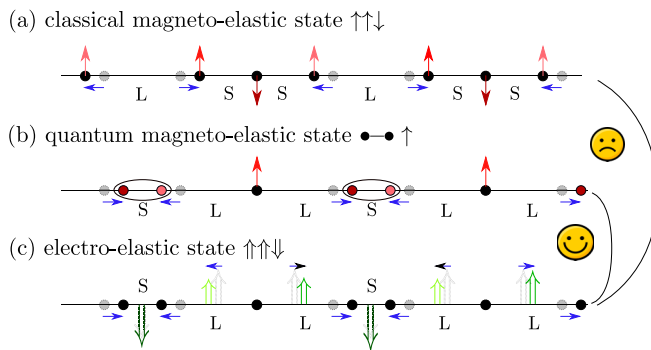

FIG. 2. Qualitative picture of magnetoelastic distortions at the classical $\uparrow\uparrow\downarrow$ and the quantum $\bullet\!-\!\bullet\uparrow$ magnetic configurations discussed in Ref. [19] [(a) and (b), respectively], and a picture of the electroelastic distortions at the dipolar $\Uparrow\Uparrow\Downarrow$ configuration (c) found in Ref. [15]. Spins are represented by single arrows in tones of red, dipoles by double arrows in tones of green. Three color tones (light, medium, dark) are used to facilitate the recognition of variables every three sites, in relation to data given below. Ionic and dipole displacements are indicated by blue arrows (nondistorted positions indicated with gray faded symbols). The size change of dipoles in (c) is demonstrative of the pantograph mechanism effect. In (a), the bond length follows a long-short-short pattern (L-S-S in the figure), providing a magnetic energy gain by getting closer (farther) antiparallel (parallel) spins. In (b), the magnetic energy gain is obtained by tightening singlet bonds following a short-long-long pattern (S-L-L in the figure). In (c), a dipolar energy gain stems from getting closer (farther) antiparallel (parallel) dipoles, with the same S-L-L bond distortions as in (b). Electroelastic distortions in (c) are compatible with the quantum magnetoelastic distortions in (b) but not with the classical ones in (a).

show that the $\Delta S^z = 1$ magnon on top of the $M = 1/3$ state fractionalizes into three $S^z = 1/3$ spatially separated solitons, where elastic distortions adapt to the magnetic order. This change in the distortion pattern induces, in the dipolar sector, a spontaneous unit polarization change which in turn fractionalizes into three sharp domain walls. This emergent magnetoelectric effect, that is, the polarization change induced by a magnetic field mediated by elastic distortions, is one of the main results in the present paper.

Both the nature of the plateau-state structure and the appearance of intertwined magnetic and electric fractional excitations, mediated by the lattice, are experimentally accessible by neutron scattering for the spin channel and by x-ray scattering for the lattice distortions. As a material potentially relevant to our discussion and findings, one should mention the monoclinic cobaltite α-CoV_2O_6 which shows a strong coupling between magnetic and dielectric order parameters together with a $M = 1/3$ magnetization plateau [20,21].

The paper is organized as follows: In Sec. II we describe the microscopic degrees of freedom, the Hamiltonian, and the parameters that define our model scenario. We also discuss the computational method. In Sec. III, we describe the double frustration effect, that is, a competition of the elastic order convenient to magnetic frustration with the elastic order driven by dipolar interactions, stressing the differences between classical and quantum regimes. We devote Sec. IV to describe the effects of increasing the magnetic field, which leads to fractional magnetic and dipolar excitations as well as localized elastic domain walls with clearly different behaviors with respect to the classical or quantum plateau state structure. Conclusions are presented in Sec. V.

II. THE MODEL SCENARIO

We briefly summarize here the model proposed in Ref. [15]. It describes spin $S = 1/2$ magnetic atoms $\boldsymbol{S}_i$ in a linear chain with elastic degrees of freedom δ_i describing the variation of the bond length between neighboring magnetic atoms $\boldsymbol{S}_i$ and $\boldsymbol{S}_{i+1}$, from a regular lattice constant length a to distorted lengths $a + \delta_i$. Electric dipolar moments p_i, normal to the chain direction, are located amid magnetic atoms $\boldsymbol{S}_i$ and $\boldsymbol{S}_{i+1}$; when the magnetic lattice is distorted the distance between dipoles p_i and p_{i+1} also changes from a to $a + \eta_i$, with $\eta_i = (\delta_i + \delta_{i+1})/2$. A fixed chain length condition is assumed, imposing a null constraint on the sum of local distortions.

To describe several materials mentioned in the Introduction, the model includes easy-axis anisotropic antiferromagnetic interactions J_1 and J_2 between nearest (NN) and next-nearest (NNN) neighbors, respectively, which produce the magnetic frustration. Electric dipoles interact via long range Coulomb interactions. Both the magnetic and dipolar sectors are coupled to the lattice in the most natural way. The spin sector does it by a standard, spin-Peierls-type, distance dependence of the NN exchange coupling linearly expanded as $J_1(i, i+1) = J_1(1 - \alpha\delta_i)$. On the other hand, the dipolar sector couples to elastic distortions through the $1/r^3$ distance dependence of long range dipole-dipole interactions and by the geometric mechanism mentioned in the Introduction, affecting the charge distribution in between magnetic

atoms as they are displaced. This so-called pantograph effect is modeled by a linear expansion of the dipole moments $p_i = p_0(1 - \beta\delta_i)\sigma_i$ where p_0 is the undistorted dipole magnitude, β measures the pantograph electro-elastic coupling and $\sigma_i = \pm 1$ is the Ising variable describing dipole orientations. The elastic distortions have an energy cost given by a stiffness constant K, providing an indirect magnetoelectric coupling. More details on the model can be found in Ref. [15].

The complete Hamiltonian reads

$$H = \sum_i [J_1(1 - \alpha\delta_i)(\mathbf{S}_i \cdot \mathbf{S}_{i+1})_\Delta + J_2(\mathbf{S}_i \cdot \mathbf{S}_{i+2})_\Delta]$$
$$+ \frac{K}{2}\sum_i \delta_i^2 + \lambda_{\text{dip}}\sum_{i<j} \frac{1}{r_{ij}^3}p_i p_j, \tag{1}$$

where $(\mathbf{S}_i \cdot \mathbf{S}_j)_\Delta$ stands for the anisotropic spin-spin product, $\lambda_{dip} > 0$ is the Coulomb coupling constant and r_{ij} is the distance between dipoles p_i and p_j, which depends on distortions. With the previous notation, expanding the dipolar $1/r^3$ dependence up to linear order in distortions and truncating up to second neighbors (see Ref. [15]), the explicit model Hamiltonian is given by

$$H = \sum_i \frac{J_1}{\Delta}(1 - \alpha\delta_i)\left(S_i^x S_{i+1}^x + S_i^y S_{i+1}^y + \Delta S_i^z S_{i+1}^z\right) + \sum_i \frac{J_2}{\Delta}\left(S_i^x S_{i+2}^x + S_i^y S_{i+2}^y + \Delta S_i^z S_{i+2}^z\right) + \frac{K}{2}\sum_i \delta_i^2$$
$$+ J_e \sum_i \left(\sigma_i\sigma_{i+1} + \frac{1}{8}\sigma_i\sigma_{i+2}\right) - J_e \sum_i \delta_i\left[\left(\beta + \frac{3}{2a}\right)(\sigma_{i-1}\sigma_i + \sigma_i\sigma_{i+1}) + \frac{1}{8}\left(\beta + \frac{3}{4a}\right)(\sigma_{i-2}\sigma_i + \sigma_i\sigma_{i+2}) + \frac{3}{16a}\sigma_{i-1}\sigma_{i+1}\right], \tag{2}$$

where $\Delta \geqslant 1$ is the easy-axis anisotropy and $J_e = \lambda_{\text{dip}}p_0^2/a^3$ is the effective dipolar interaction coupling, (J_1, J_2, and J_e in energy units). Magnetic couplings J_1 and J_2 are divided by Δ to reach the Ising regime in the highly anisotropic $\Delta \to \infty$ limit.

Following Ref. [15], we are interested on a parameter region where the magnetic and dipolar couplings are of the same order of magnitude, so both the spin and dipole configurations are relevant to determine the ground state of the system. Also the magnetoelastic coupling α and the electroelastic coupling β are similar to provide an efficient elastically mediated magnetoelectric interaction. We then avoid the multiplicity of parameters in the Hamiltonian Eq. (2) by taking Ka^2 as the energy unit and fixing J_1, J_e, α, and β at convenient values detailed below. Only J_2 and Δ will be varied to explore the incidence of magnetic frustration and easy-axis anisotropy (measured as $\gamma = 1/\Delta$ in Ref. [15]) in the ground-state properties of the system. Different values of J_1, J_e, and β can be studied similarly.

External electric and magnetic fields $\mathbf{E}$ and $\mathbf{B}$ will be adjusted to drive the system to the peculiar double frustration scenario we discuss in the present paper. This is the region where the electric field polarizes the otherwise antiferroelectric dipolar sector (driven by J_e) up to 1/3 of saturation, provoking the period three $\Uparrow\Uparrow\Downarrow$ dipolar pattern (see Fig. 3 in Ref. [15]) and the magnetic field sets the spin degrees of freedom in the $M = 1/3$ plateau region (see Fig. 6 in Ref. [15]). For a magnetoelastic, spin-Peierls, chain (not coupled to electric dipoles), this plateau is known to appear together with an energetically favorable period-three elastic distortion [22–24]. On the other hand, for the electroelastic chain obtained from the Hamiltonian Eq. (2) when the spin sector is decoupled ($\alpha = 0$), the $\Uparrow\Uparrow\Downarrow$ dipolar pattern also comes along with period-three elastic distortions (as discussed in Ref. [15]), bringing closer (farther) antiparallel (parallel) dipoles. This situation might be reversed, for instance, in the presence of itinerant electrons, since they may induce RRKY-like interactions between dipoles leading to ferroelectric effective couplings (see, e.g., Ref. [25]).

The question arises whether the elastic distortions compete or collaborate in lowering the ground-state energy of the magneto-electro-elastic multiferroic system. We show below that they do compete, with profound consequences both in the magnetic plateau configuration and the magnetic excitations at the high field border of the plateau.

Our results are based on extensive numerical computations following an iterative self-consistent method [26] where the spin sector is solved exactly by density matrix renormalization group (DMRG) techniques [27]. At each iteration, for a given configuration of dipoles $\{\sigma_i\}$ and a quantum state for the spins $\{\mathbf{S}_i\}$, the lattice distortions δ_i are obtained by minimizing the elastic energy under a fixed chain length condition. Unconstrained distortions δ_i^{free} are computed through the local zero gradient conditions,

$$K\delta_i^{\text{free}} = \alpha J_1/\Delta\left\langle\left(S_i^x S_{i+1}^x + S_i^y S_{i+1}^y + \Delta S_i^z S_{i+1}^z\right)\right\rangle$$
$$+ J_e\left(\beta + \frac{3}{2a}\right)(\sigma_{i-1}\sigma_i + \sigma_i\sigma_{i+1})$$
$$+ \frac{1}{8}J_e\left(\beta + \frac{3}{4a}\right)(\sigma_{i-2}\sigma_i + \sigma_i\sigma_{i+2})$$
$$+ J_e\frac{3}{16a}\sigma_{i-1}\sigma_{i+1} - \beta\varepsilon\sigma_i, \tag{3}$$

where $\epsilon = 2p_0 E$ is the normalized electric field, while the constraint is imposed as

$$\delta_i = \delta_i^{\text{free}} - \overline{\delta^{\text{free}}}, \tag{4}$$

where the bar stands for average value along the chain. Dipolar configurations $\{\sigma_i\}$ close to the electroelastic sector solution are then compared.

Interestingly, the self-consistent conditions in Eqs. (3) and (4) also allow for a qualitative analysis of the influence of spin-spin and dipole-dipole correlations on the elastic distortions.

III. DOUBLE FRUSTRATION EFFECT

A. Qualitative description

The elastic distortions associated with the $M = 1/3$ magnetic plateau configuration and those associated with the $\Uparrow\Uparrow\Downarrow$ dipolar pattern can be qualitatively described considering the NN interactions in Eqs. (3) and (4). We then provide the numerical evidence for the outcoming picture in the following subsection.

$M = 1/3$ magnetic plateaus come in two flavors, dubbed classical and quantum [19]. In the so-called classical plateau, spin components parallel to the magnetic field have a nonvanishing $\langle S_i^z \rangle$ expectation value in an ordered pattern with two positive, one negative terms that we represent by $\uparrow\uparrow\downarrow$. These expectation values are reduced by quantum fluctuations in the isotropic $\Delta = 1$ case, but approach ± 0.5 in the highly easy-axis anisotropic case $\Delta \gg 1$. Spin-spin correlations $\langle \mathbf{S}_i \cdot \mathbf{S}_{i+1} \rangle$ are positive between ferromagnetic (parallel) neighbors $\uparrow\uparrow$ and negative between antiferromagnetic (antiparallel) neighbors $\uparrow\downarrow$ and $\downarrow\uparrow$, approaching the Ising correlations ± 0.25 for $\Delta \gg 1$. From Eq. (3), the correlation $\langle \mathbf{S}_i \cdot \mathbf{S}_{i+1} \rangle$ affects the bond distortion δ_i; the $\uparrow\uparrow\downarrow$ spin configuration favors distorted long bonds between ferromagnetic neighbors and short bonds between antiferromagnetic neighbors, that is, a L-S-S distortion pattern [see Figs. 1 and 2(a)]. Notice that the antiferromagnetic coupling $J_1(1 - \alpha\delta_i)$ gets stronger for satisfied antiferromagnetically aligned neighbors and weaker for frustrated ferromagnetically aligned neighbors.

In contrast, in the so-called quantum plateau two neighboring spins (out of three) tend to form singlets while the third one points up, in a configuration that we represent by $\bullet\!-\!\bullet \uparrow$ [see Fig. 2(b)]. In an ideal case, the spins forming a quantum singlet would have $\langle S_i^z \rangle = 0$ and the third one $\langle S_i^z \rangle = 0.5$, with singlet correlation $\langle \mathbf{S}_i \cdot \mathbf{S}_{i+1} \rangle = -0.75$ and vanishing correlation between the spin up and its neighbors; the real situation may be characterized as a quantum plateau when the spin expectation and spin-spin correlation values show a tendency to such pattern. Again, from Eq. (3), one can see that a very negative singletlike correlation strongly favors a short bond at the expense of long bonds [according to Eq. (4)] where spin correlations are close to zero, giving rise to a short-long-long (S-L-L) distortion pattern. Notice that the singlets are more likely to appear in the isotropic case $\Delta = 1$, while the easy-axis anisotropy $\Delta > 1$ diminishes transverse correlations and favors the classical configuration.

In turn, the NN dipolar correlations are related to lattice distortions through the second line of Eq. (3): Bond distortion δ_i is influenced by the correlations of the dipole σ_i located at bond i with NN dipoles at both sides. The $\Uparrow\Uparrow\Downarrow$ configuration then favors short bonds where the dipole $\Downarrow$ is located, at the expense of generating long bonds where the dipoles point $\Uparrow$ to fulfill the constraint in Eq. (4), preferring to induce a S-L-L distortion pattern [see Fig. 2(c)]. Recalling that dipoles always remain midway between adjacent magnetic atoms, in terms of dipole positions these magnetic lattice distortions make antiparallel dipoles get closer and parallel dipoles get further away. The NNN dipolar interactions, necessary to introduce the $\Uparrow\Uparrow\Downarrow$ order in the electroelastic phase diagram (as discussed in Ref. [15]), enter in Eq. (3) with smaller coefficients. From this qualitative discussion, the electroelastic dipolar

configuration $\Uparrow\Uparrow\Downarrow$ found in Ref. [15] is compatible with the quantum magnetic plateau configuration but competes with the classical plateau configuration, which is usually the one observed in homogeneous $J_1 - J_2$ magnetically frustrated spin chains in a wide variety of regimes (isotropic with [22,23] and without [18] elastic coupling, anisotropic [28]). Then, the coupling to dipolar degrees of freedom through lattice distortions introduces a second frustration mechanism. Our numerical analysis below provides clear surprising effects due to this double frustration scenario. In a regime of low anisotropy and high magnetic frustration, favoring quantum fluctuations, this second frustration is responsible for the stabilization of a quantum $M = 1/3$ plateau state. In contrast, for higher easy-axis anisotropy and/or lower magnetic frustration, the second frustration competition leads to a spontaneous parity symmetry breaking in the classical $M = 1/3$ plateau state.

B. Numerical DMRG analysis

We have performed an extensive numerical computation of the ground state of the model in Eq. (2), in the presence of magnetic and electric fields driving the system to magnetization $M = 1/3$ and polarization $P = 1/3$. To evaluate the role of magnetic frustration and easy-axis anisotropy, we explored the $J_2/J_1 - \Delta$ plane, fixing the remaining parameters at $J_1 = 0.5Ka^2$, $J_e = 0.2Ka^2$ and $\alpha = \beta = 0.2$ with $K = a = 1$; correspondingly, the electric field is taken as $\epsilon = 0.16$ (see Fig. 3 in Ref. [15]).

The ground state is found through an iterative numerical analysis based on DMRG to solve the magnetic sector in the adiabatic Eq. (3), along the lines stated in Ref. [26] and implemented in a similar context in Refs. [15,16]. At each point chosen in the $J_2/J_1 - \Delta$ plane, the ground state of the system is found as follows: starting from the δ_i and σ_i configuration that solves the electroelastic part of the Hamiltonian, the quantum ground state of the spin system is obtained by the DMRG algorithm. Therefore, we reobtain the set of δ_i from Eqs. (3) and (4) and prove different σ_i to minimize the total energy, until convergence. We use periodic boundary conditions and we have kept the truncation error less than $O(10^{-12})$, during up to more than 100 sweeps in the worst cases. This assures that errors of the DMRG computation are smaller than symbol sizes in each figure. The DMRG computations were implemented using the ITensor software library [29].

We have covered a wide region of the $J_2/J_1 - \Delta$ plane. From this exploration, we found distinct regimes that we describe below. We paid attention to the isotropic case $\Delta = 1$, mainly for theoretical reasons, and to high values of Δ where one expects a classical behavior which may be in closer relation to real materials. Regarding the frustration ratio J_2/J_1, we distinguish moderate and highly frustrated values (see Fig. 6 in Ref. [15]). Representative selected points are:

(i) $\Delta = 1$, $J_2/J_1 = 0.5$. Due to the isotropic Heisenberg interaction and the high magnetic frustration ($J_2/J_1 = 0.5$ is the maximally frustrated point in the case of Ising interactions) quantum fluctuations are enhanced at this point.

(ii) $\Delta = 4$, $J_2/J_1 = 0.8$. Easy-axis anisotropy and low magnetic frustration inhibit quantum fluctuations, favoring classical behavior.
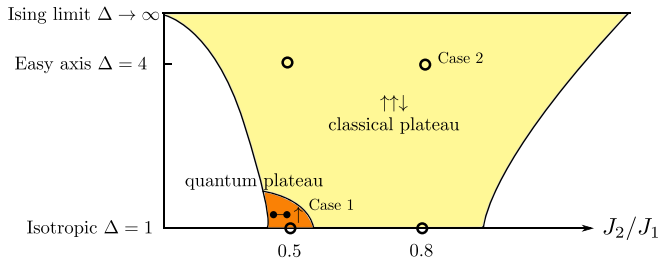
FIG. 3. Schematic phase diagram in the frustration ratio (J_2/J_1) and the easy-axis anisotropy (Δ) plane. The colored regions indicate the parameter regimes where $M = 1/3$ plateaus are observed in magnetization curves. The robust magnetic order giving rise to the plateau is mostly a collinear $\uparrow\uparrow\downarrow$ classical structure (yellow region) but turns into a quantum $\bullet\!-\!\bullet\uparrow$ state (orange region) when high frustration and low anisotropy enhance the quantum fluctuations. The circles mark the four points detailed in this paper (unnumbered ones are described in Supplemental Material [30]).

(iii) $\Delta = 1$, $J_2/J_1 = 0.8$. Selected as a point with isotropic Heisenberg interaction and low frustration.

(iv) $\Delta = 4$, $J_2/J_1 = 0.5$. Selected as a high magnetic frustration poinmagnetic dipole energyt, with weaker transverse spin interactions softening quantum fluctuations.

We found important qualitative differences between the first case (case 1 in the following) and the others. For this reason, we provide details on that and the second one (case 2 in the following) and defer the others for Supplemental Material [30]. Our complete analysis leads to the schematic phase diagram shown in Fig. 3. A characterization of the phase boundaries is an interesting question but is out of the scope of the present paper.

We have checked at each of these points that the magnetization curves indeed show plateaus at $M = 1/3$, with different widths. For cases 1 and 2, these are shown in Figs. 4(a) and 4(d).

1. Case 1 ($\Delta = 1$, $J_2/J_1 = 0.5$)

We have found that the *double frustration* caused by the dipolar degrees of freedom is able to radically change the otherwise classical magnetic plateau structure to a quantum one. This is a manifestation of a *strong magnetoelectric effect*. The local profile of the relevant variables has been computed in a chain of $N_s = 174$ sites, with periodic boundary conditions and a magnetic field $h_z = 0.6$, setting $M = 1/3$ (meaning $S_{\text{total}}^z = (N_s \times \frac{1}{2})/3$).

The local results show a repeated structure every three sites, as expected; a detail of a portion of the chain is shown in Fig. 4(b). We have used three color tones (light-medium-dark) to identify the corresponding period-three sublattices. We have also drawn vertical lines in these plots to indicate the magnetic sites, drawing site variables ($\langle S_i^z \rangle$) markers upon these lines and bond variables (δ_i, p_i and spin-spin correlations) markers between them. One can see in the sequence of $\langle S_i^z \rangle$ (red circles in the upper plot, with light-medium-dark tones every three sites) a repetition of one spin up ($\langle S^z \rangle \approx 0.4$, in medium red) followed by two spins with almost vanishing expectation value ($\langle S^z \rangle \approx 0$, in dark and light red). The NN spin correlations (red diamonds

in the lower plot, with corresponding light-medium-dark tones every three bonds) take a very negative value (below -0.6) every three bonds, indicating the tendency to form two sites local quantum singlets just between sites with almost vanishing $\langle S^z \rangle$, with low antiferromagnetic correlations between them and sites with spin up. The longitudinal and transverse correlations are shown with up-triangles and horizontal-triangles for more detail: typical singlet correlations (in dark red) get equal contributions from each spin component $\langle S_i^x S_{i+1}^x \rangle = \langle S_i^y S_{i+1}^y \rangle = \langle S_i^z S_{i+1}^z \rangle \approx -0.2$, while the other bonds show almost uncorrelated z components $\langle S_i^z S_{i+1}^z \rangle \approx 0$. The elastic distortions (blue squares in the upper plot, also with light-medium-dark tones) are negative in the dark bonds and positive in the rest, forming a S-L-L bond distortion pattern. The magnetic ions in the spin quantum singlets get closer, augmenting the spin exchange $J_1(1 - \alpha\delta_i)$ for better magnetic energy gain at the expense of elastic energy cost. These together are clear signals of the $\bullet\!-\!\bullet\uparrow$ quantum plateau structure [see Fig. 2(b), where the same tones of red are used for spin sites]. The $\uparrow\uparrow\downarrow$ dipole amplitudes (green diamonds in the upper plot) pin the dipoles pointing down in the short bonds; this makes antiparallel dipoles get closer and parallel dipoles get farther, in a pattern that minimizes the electro-elastic energy [see Fig. 2(c), where the same tones of green are used for dipoles]. The same elastic distortions thus contribute to the gain of both electric and magnetic energy. The ground state obtained in case 1 may be visually summarized in the cartoon description provided in Fig. 4(c).

Notice that this state breaks the translation invariance of the Hamiltonian in Eq. (2) but maintains the inversion symmetry with respect to spin up sites or dipole down bonds (in contrast to case 2 discussed below). As a consequence, the ground state is threefold degenerate.

One should recall that a different (classical) magnetic order has been previously observed at the $M = 1/3$ plateau of the isotropic, frustrated $J_1 - J_2$ antiferromagnetic-elastic spin $S = 1/2$ chain [23] in the absence of local dipoles. We can say that the distortions associated to the dipolar order dominate and destroy the otherwise collinear $\uparrow\uparrow\downarrow$ classical magnetic plateau order of the isotropic, frustrated $J_1 - J_2$ antiferromagnetic-elastic spin chain. Instead they give rise to a $\bullet\!-\!\bullet\uparrow$ quantum magnetic plateau order, elastically compatible with the dipolar order, where the formation of spin quantum singlets lowers the magnetic energy. This is one of the main results in this paper.

2. Case 2 ($\Delta = 4$, $J_2/J_1 = 0.8$)

In the anisotropic, less-frustrated case, we have observed qualitatively different magnetic and electric orders, again with a period-three structure. Numerical results are shown in Fig. 4(e) together with the corresponding cartoon picture in Fig. 4(f).

The spins clearly adopt the $\uparrow\uparrow\downarrow$ classical plateau structure. This is seen in the sequence of $\langle S_i^z \rangle$ with two positive, one negative values close to 0.5 (red circles in the upper plot) and mainly in the almost vanishing transverse correlations $\langle S_i^+ S_{i+1}^- \rangle$ (horizontal-triangles in the lower plot); longitudinal correlations close to $0.25 (-0.25)$ (up-triangles in the lower
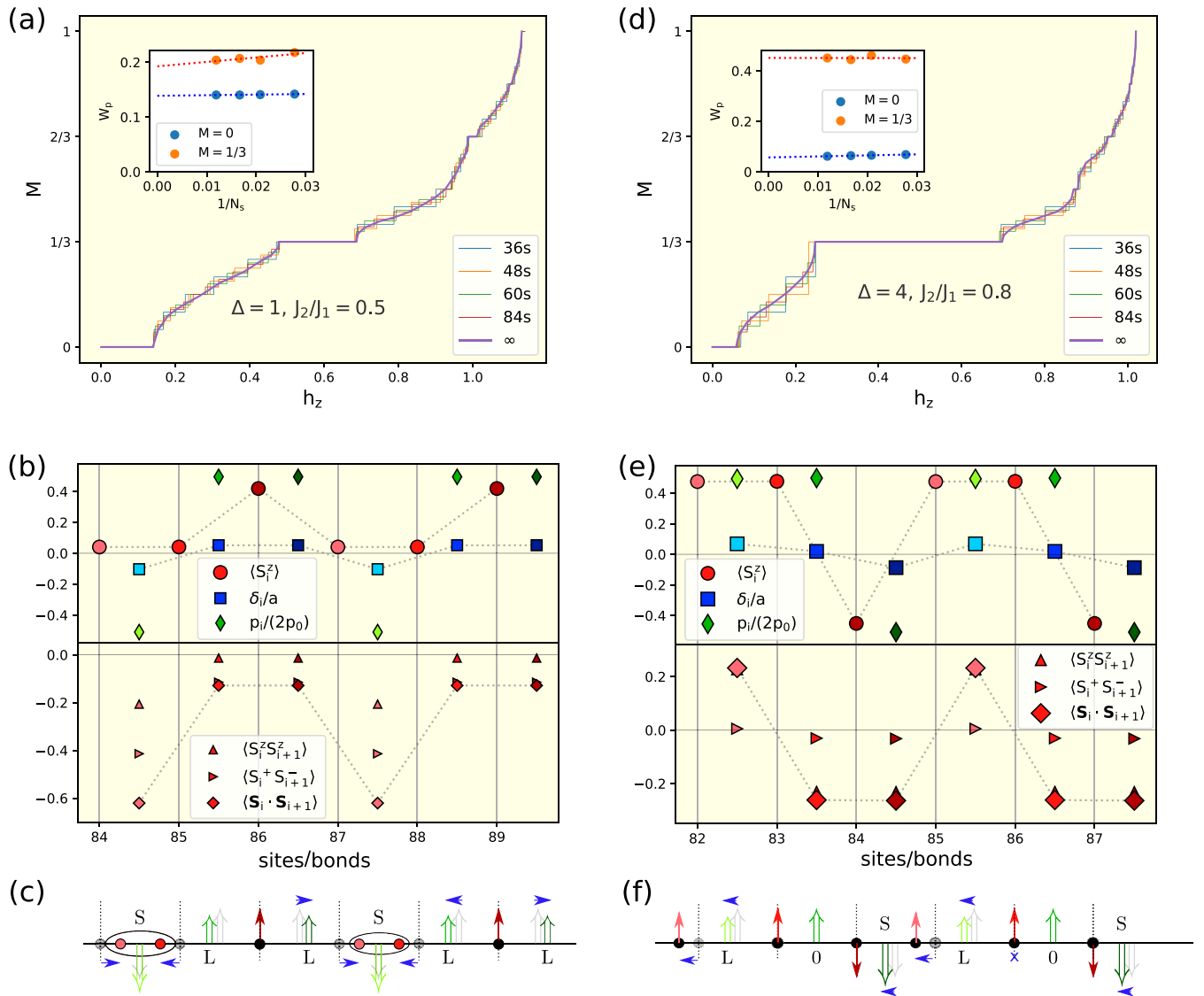
FIG. 4. (a), (d) Magnetization curves M versus. $h_z = g\mu_B|\boldsymbol{B}|$ (g being the gyromagnetic ratio of the electron in the specific material and μ_B the Bohr magneton) showing the existence of the $M = 1/3$ plateau in cases 1(a) and 2(b) discussed in detail in this paper. The widths W_p of the main magnetization plateaus are computed for several finite chain lengths and extrapolated to infinite size as shown in the insets. The smooth lines suggest the magnetization curves in the thermodynamic limit. For case 1, the plateau is narrower than case 2, due to the enhancement of quantum fluctuations favored by isotropic interactions and high magnetic frustration.(b), (c) Local profile of site and bond observables in the $M = 1/3$ state for $\Delta = 1$, $J_2/J_1 = 0.5$ (case 1), obtained with the self-consistent numerical computations; a section of six sites (indicated by vertical lines) is taken from the $L = 174$ chain with periodic boundary conditions. In the upper plot, different light-medium-dark tones are used to emphasize the period three structure of the spin expectation values $\langle S_i^z \rangle$ (in units of $\hbar$, in red circles), the bond distortions δ_i (in units of the lattice constant a, in blue squares drawn between sites) and dipolar moments p_i (divided by $2p_0$, in green thin-diamonds between sites). The lower plot shows the nearest-neighbor spin correlations $\langle \boldsymbol{S}_i \cdot \boldsymbol{S}_{i+1} \rangle$ in red diamonds; a detail of longitudinal $\langle S_i^z S_{i+1}^z \rangle$ and transverse $\langle S_i^+ S_{i+1}^- \rangle = \langle S_i^x S_{i+1}^x \rangle + \langle S_i^y S_{i+1}^y \rangle$ correlations is given in triangles. Data shows the formation of local quantum singlets alternating with partially decoupled spins up every three sites. The cartoon picture in (c) qualitatively collects these numerical results and shows the compatibility of the short-long-long (S-L-L) quantum magnetoelastic and electroelastic patterns in Fig. 2. (e), (f) The $M = 1/3$ ground state for $\Delta = 4$, $J_2/J_1 = 0.8$ (case 2). Symbols and colors follow the conventions in (b). Spin data shows the classical $\uparrow\uparrow\downarrow$ plateau features, with $\langle S_i^z \rangle$ not reaching ± 0.5 because of small quantum fluctuations. Although the spin structure is classical, the elastic distortions do not fit the classical magneto-elastic pattern in Fig. 2 but the long-null-short (L-0-S) sequence depicted qualitatively in (f). The interaction between dipoles and spins, mediated by distortions, frustrates the magnetoelastic order producing the breaking of inversion symmetry.

plot) correspond to collinear parallel (antiparallel) spins. In this state, the magnetic sector could be well described by classical Ising spins, neglecting the quantum fluctuations. However, we find in the next section that the magnetic

excitations above this plateau state show a clear quantum behavior.

Note that the lattice distortions do not follow the pattern of the magnetic correlations [compare with Fig. 2(a)]. The

first-neighbor dipolar terms in the self-consistent Eq. (3), following the $\Uparrow\Uparrow\Downarrow$ configuration induced by the external electric field [see Fig. 2(c)], are not compatible with such magnetic correlations and force a competition in determining the lattice distortions. The resulting distortion pattern does neither optimize the magnetic energy nor the dipolar energy separately, but their sum with the elastic energy. It can be qualitative described as long-null-short (L-0-S) distortion pattern [following light-medium-dark blue squares in the upper plot of Fig. 4(e)]. A different, degenerate, ground state is obtained by inversion with respect to any of the short bonds. Thus the ground state is sixfold degenerate.

The features of the ground state in case 2 may be recognized in the cartoon in Fig. 4(f). The double frustration effect leads to a compromising distortion pattern that breaks the inversion symmetry. This lack of inversion symmetry in the distortion pattern of course modifies the magnetic and dipolar couplings through the magnetoelastic coupling α and the pantograph electroelastic coupling β. As a consequence, the spins (dipoles) pointing up have slightly different values of $\langle S^z \rangle$ (p_i), breaking the inversion symmetry observed in the quantum plateau case 1 and also in the $J_1 - J_2$ magnetoelastic spin chain [23]. This spontaneous symmetry breaking is another important result, a consequence of the present double frustration effect. Were charge degrees of freedom included, the induced charge order would result in a longitudinal component of electrical polarization [2].

The analysis of the other points indicated in Fig. 3 show a classical plateau behavior similar to that observed in case 2. They correspond to isotropic spin interactions and low frustration ($\Delta = 1$, $J_2/J_1 = 0.8$) and to a highly frustrated case with important easy-axis anisotropy ($\Delta = 4$, $J_2/J_1 = 0.5$). It appears that both isotropy and high frustration are necessary to stabilize the quantum plateau. Further numerical exploration indicates that there is a finite small region around $\Delta = 1$, $J_2/J_1 = 0.5$ where the $M = 1/3$ plateau remains open and the spins order in the quantum $\bullet\!-\!\bullet\uparrow$ structure, as shown schematically in Fig. 3.

As a summary of this section, we have provided a qualitative description and numerical evidence for a double frustration effect in a multiferroic model scenario.

IV. COMPOSITE EXCITATIONS INDUCED BY A MAGNETIC FIELD

The $\Delta S^z = 1$ spin excitations induced by a magnetic field on a plateau state are the key to understand the high field plateau border. It is well-known that the excitation of the $M = 0$ plateau in one-dimensional antiferromagnetic spin chains is not a stable singlet-triplet excitation but decays into two spinons [26,31–34]. Each spinon carries spin $S^z = 1/2$ as a topological charge and may be described as a soliton quasiparticle interpolating between different dimerized vacua; spatially, the soliton profile can be seen as a smooth domain wall. We have discussed this spin fractionalization phenomenon in the present multiferroic model in Ref. [15].

The $\Delta S^z = 1$ spin excitations on top of the $M = 1/3$ magnetization plateau in antiferromagnetic magnetoelastic spin chains is also known to exhibit spin fractionalization [23]. Remarkably, this goes beyond the spinon description: the

excitation decays into three $S^z = 1/3$ noninteracting solitonic excitations (dubbed tertions). For a classical $\uparrow\uparrow\downarrow$ plateau, it has been shown that the tertions have a local singlet core causing the $\uparrow\uparrow\downarrow$ order on one side to be shifted by one site with respect to the other side. In this way, the tertion interpolates between two different $\uparrow\uparrow\downarrow$ domains.

It has been observed in several systems that the high-field plateau border is characterized by a sudden finite magnetization jump when the magnetic field takes a threshold value. The magnetization curves in Fig. 4 suggest that this might also occur in our model. If this is the case, the magnetic excitation would fractionalize into a periodic lattice of self-avoiding solitons [33,35]. Such a periodic magnetic structure could be detected by unusual line shapes in neutron-scattering data [36], as well as the associated lattice distortions could be detected by x-ray measurements.

A natural question arises, whether these features are modified by the double frustration effect in the present magneto-electro-elastic chain. We have explored the numerical self-consistent solutions of Eqs. (3) and (4) in periodic chains with N_s sites in the subspace of $S_{\text{total}}^z = (N_s \cdot \frac{1}{2})/3 + 1$ (that is, one unit of magnetization above $M = 1/3$). We considered large chains to allow for a most clear spatial separation of the three expected tertions. We report results on chains of $N_s = 174$ sites,[1] where the plateau state has $S_{\text{total}}^z = 29$ and the excited state has $S_{\text{total}}^z = 30$.

In the present multiferroic model scenario, we have confirmed that the $\Delta S^z = 1$ excitation induced by a magnetic field on top of the $M = 1/3$ state indeed fractionalizes into three $S^z = 1/3$ spatially separated tertions. The trial of different dipolar configurations has shown that the dipolar sector suffers a spontaneous unit polarization change along the electric field direction to minimize the energy cost of the distortions accompanying the magnetic order. This polarization change induced by a magnetic field is an emergent magnetoelectric effect mediated by elastic distortions. We discuss below the numerical data supporting these statements.

A. Case 1

We show in Fig. 5 numerical results for the magnetically excited state in the isotropic frustrated regime ($\Delta = 1$, $J_2/J_1 = 0.5$). Using the same color codes as in the plateau state [see Fig. 4(b)], in the upper panel we show the local $\langle S_i^z \rangle$ in red circles, the dipoles p_i in green diamonds and the distortions δ_i in blue squares; the light-medium-dark tones for sites 1–3 are repeated every three sites to visually distinguish the associated sublattices. In the lower panel, we show the $\langle \mathbf{S}_i \cdot \mathbf{S}_{i+1} \rangle$ correlations. With the help of the color tones, one can see a short wavelength oscillation of each observable, with period three as in the plateau state, but modulated by a long wavelength oscillation spanning three whole periods along the chain. The regions around sites ~ 26 (marked as I in the plots), $\sim 26 + N_s/3 = 84$ (marked as II in the plots), and $\sim 26 + 2 \times N_s/3 = 142$ show locally the same features

---

[1]For a periodic pattern with magnetization $S_{\text{total}}^z = (N_s \cdot \frac{1}{2})/3 + 1$ to be commensurate with the chain length, N_s must be restricted to integers of the form $9q + 3$ [23].
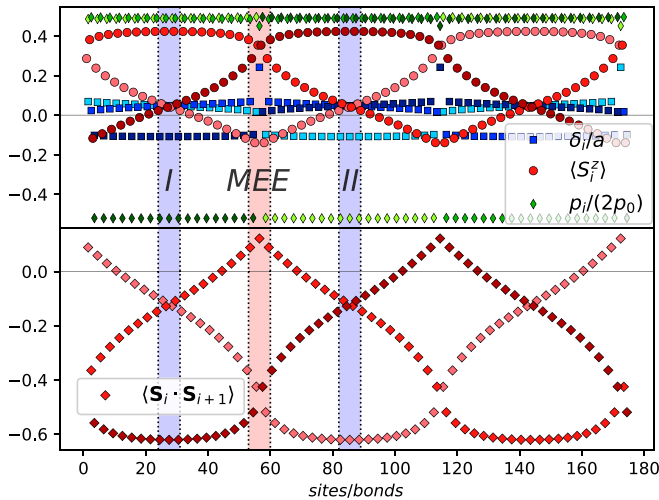
FIG. 5. (See online version to appreciate details.) Magneto-electro-elastic excitations (MEE) with $\Delta S^z = 1$ induced by the magnetic field on top of the $M = 1/3$ plateau for $J_2/J_1 = 0.5$, $\Delta = 1$ (case 1). In the top panel, we show numerical results for the local observables (upper plot) and spin correlations (lower plot). Symbols and colors follow the conventions in Fig. 4(b). The magnetic sector shows regions which adopt the ●—● ↑ quantum plateau order (two of them highlighted as *I* and *II*), interpolated by soliton structures with a classical ↓↑↑↓ center. The position of the ●—● ↑ pattern is shifted to a different sublattice across each soliton. Dipolar domain walls ⇓⇑⇑⇑⇓ are formed at the core of the magnetic solitons, shifting the ⇑⇑⇓ order from one to another sublattice to accompany the magnetic configuration; these dipolar domain walls carry fractionalized spontaneous electric excitations. The lattice distortions also accompany the magnetic configuration but show singular localized excitations at each dipolar domain wall. Each region between ●—● ↑ quantum plateau orders thus allocates a coupled magneto-electro-elastic excitation (the one between regions *I* and *II* is highlighted as MEE in the plots). A cartoon picture of these results is shown in Fig. 6.

as the plateau state. However, in the first one the spin up is located on the medium-red sublattice (region *I*), in the second one it falls on the dark-red sublattice (region *II*) and in the third region it corresponds to the light-red sublattice. Thus, regarding the spin sector, each of these regions adopts one of the three degenerate possible quantum plateau configurations, different because of a relative shift of the spin up and the spin singlet positions by one site to the right. In the sites between the plateau regions, one can see a smooth sublattice interpolation between observables; for instance, the $\langle S_i^z \rangle$ in the

medium-red sublattice evolves from a spin up in region *I* to a spin in a singlet in region *II*. These intermediate sites then allocate the solitonic excitations interpolating between different vacua (in the sense of degenerate plateau states related by translations); the analysis of local $\langle S_i^z \rangle$ values shows that they carry a fraction $S^z = 1/3$ of the magnetic excitation. At the center of the soliton, the spins take a ↓↑↑↓ configuration, that may be called a classical core between quantum orders. One can of course notice that the soliton regions occupy an important fraction of the chain length. As the spatial width of the magnetic solitons is usually in inverse relation with the plateau width (or the spin gap producing it [26]), we expect that in a larger chain they will maintain their size and more space will be left for better defined plateau regions. The analysis of dipolar configurations necessary to minimize the system energy has shown that the dipolar order ⇑⇑⇓ induced by the electric field (fixed at the plateau value $\epsilon = 0.16$) is altered by the appearance of three dipolar domain walls with patterns ⇓⇑⇑⇑⇓. Each of them can be seen as the insertion of an extra ⇑ dipole, namely, a dipolar excitation. As the three domain walls accumulate one dipole flip with respect to the homogeneous ⇑⇑⇓ order, we observe a spontaneous unit dipolar excitation that appears to decay into three domain walls. A similar behavior is reported in Ref. [28] for magnetic excitations above the $M = 1/3$ plateau in the Ising limit. These dipolar excitations are localized at the soliton cores, so the dipolar order observed at the plateau state is shifted by one site at each domain wall accompanying the shift of magnetic plateau structures. Notice that magnetic tertions and dipolar domain walls occur in the same positions, a fact that may be interpreted as a magnetoelectric coupling between magnetic and dipolar excitations.

The elastic sector evolves smoothly along the magnetic solitons, shifting the S-L-L pattern by one site as the spins and dipoles do, with a noticeably exception at the dipolar domain walls. A singularly long bond is formed there, while the others abruptly interchange from null to short. We interpret this feature as a local elastic excitation, coupled to the magnetoelectric one. Thus a localized magneto-electro-elastic excitation (indicated as MEE in Fig. 5) shows up between quantum plateau regions.

A cartoon picture of these features is drawn in Fig. 6. The spins, dipoles, and distortions are schematically indicated at the quantum plateau regions *I* and *II* (as labeled in Fig. 5), separated by the MEE excitation with a classical magnetic ↓↑↑↓ core coinciding with the ⇓⇑⇑⇑⇓ dipolar domain wall.
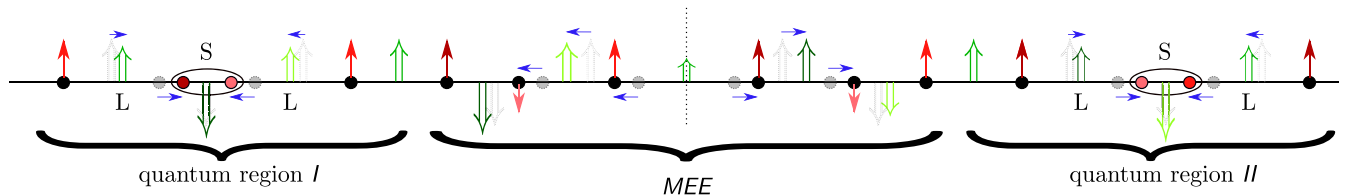

FIG. 6. Qualitative picture of the magneto-electro-elastic (MEE) excitation separating the quantum plateau regions *I* and *II* in Fig. 5. The excitation has a classical magnetic ↓↑↑↓ core coinciding with the ⇓⇑⇑⇑⇓ dipolar domain wall and a highly enlarged bond. Local observables and color codes follow actual data in the upper plot in Fig. 5. The dotted line is a mirror plane showing the parity symmetry of the MEE excitation. The local order in quantum region *II* is shifted by one site with respect to the order in quantum region *I*.
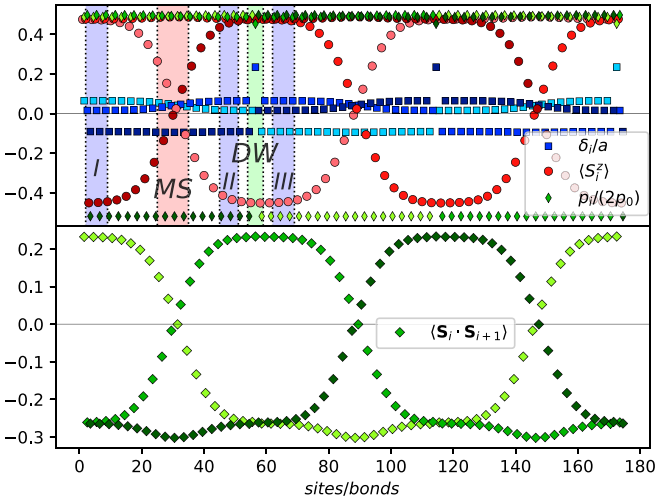
FIG. 7. (See online version to appreciate details.) Decoupled electroelastic and magnetic and excitations with $\Delta S^z = 1$ induced by the magnetic field on top of the $M = 1/3$ plateau for $J_2/J_1 = 0.8$, $\Delta = 4$ (case 2). The plot in the upper panel shows the local observables, that in the lower panel shows spin correlations. Magnetic solitons (one of them labeled as MS in the figure) having a singlet core interpolate between different classically $\uparrow\uparrow\downarrow$ ordered regions related by one-site translations (see, for instance, regions *I* and *II* in the figure). Dipolar excitations in the form of domain walls $\Downarrow\Uparrow\Uparrow\Uparrow\Downarrow$ (DW), accompanied by localized elastic excitations, are spatially decoupled from the magnetic solitons. They separate different mirror-related classically $\uparrow\uparrow\downarrow$ ordered regions (see, for instance, *II* and *III*). All of the six degenerate magneto-electro-elastic classical plateau configurations show up in different regions of the system. A cartoon picture of these results is shown in Fig. 8.

B. Case 2

In Fig. 7, we show the results obtained for the excitations of the classical plateau state in the anisotropic less frustrated regime $J_2/J_1 = 0.8$, $\Delta = 4$, which are qualitatively different from case 1. Here the magnetic sector, in the $S^z_{\text{total}} = (N_s \cdot \frac{1}{2})/3 + 1$ excited subspace, presents three regions with each $\uparrow\uparrow\downarrow$ classical plateau order, periodically modulated along the chain. In each classical plateau region, the $\uparrow\uparrow\downarrow$ pattern lies in different sublattices (for instance, regions *I* and *II* in the figure), separated by solitons [one is highlighted as a magnetic soliton (MS) in the plot]. Again these solitons are tertions, carrying a fraction $S^z = 1/3$ of the magnetic excitation. They interpolate classical plateau regions, having a local quantum spin singlet core; the same features have been observed in the excitations of the $M = 1/3$ classical plateau in magnetoelastic chains, in the absence of dipolar degrees of freedom [23]. In addition, the solitons are narrower than in case 1, in accordance with a wider magnetic plateau (see Fig. 4).

The dipolar sector again presents a unit spontaneous excitation (dipole flip) fractionalized into three domain walls (one of them is highlighted as DW in the plot). But in this case, the domain walls appear to decouple from the magnetic solitons. Instead, they occur inside a $\uparrow\uparrow\downarrow$ plateau region signaling a parity change of the accompanying lattice distortions (see, for instance, the regions highlighted as *II* and *III* in the plot, with mirror symmetry with respect to the domain wall between them). Singular elastic excitations (very long bonds) show up together with the dipolar domain walls. One can thus observe electroelastic excitations well decoupled from magnetic $S^z = 1/3$ excitations.

As the dipolar domain walls separate the two parity-related degenerate elastic configurations compatible with the same
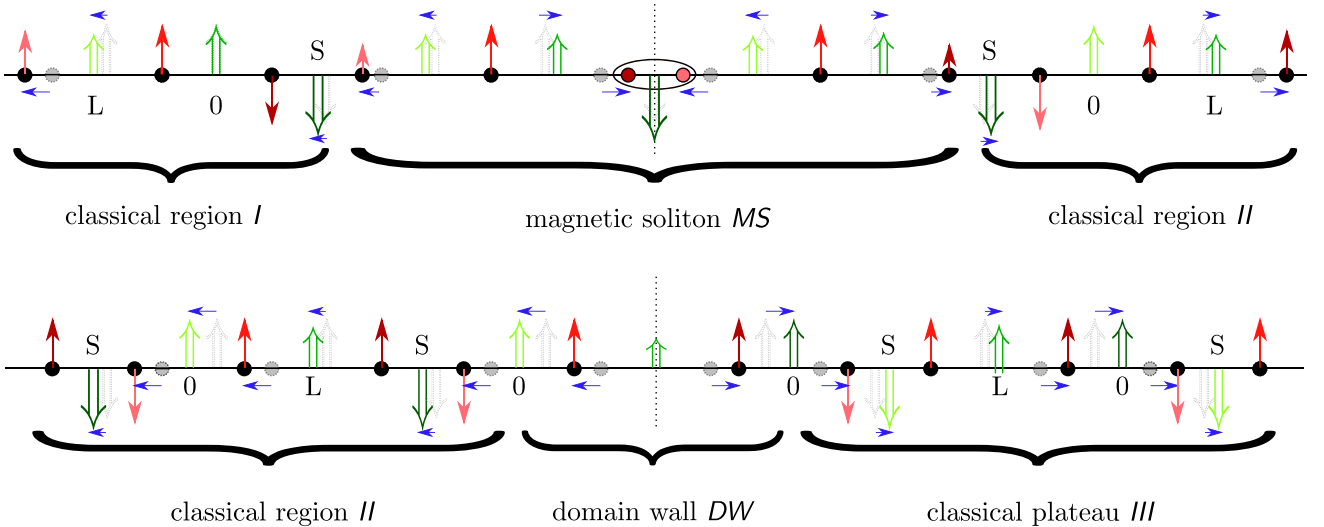

FIG. 8. Qualitative picture of the magnetoelastic and electroelastic excitations in Fig. 7. The cartoon in the upper panel describes the magnetoelastic solitonic excitation MS with a quantum singlet core interpolating the classical orders highlighted as *I* and *II* in Fig. 5; in passing the soliton, the L-0-S distortion pattern changes to S-0-L and the $\uparrow\uparrow\downarrow$ magnetic pattern is shifted by one site while the dipolar $\Uparrow\Uparrow\Downarrow$ pattern remains unaltered. In the lower panel, the electroelastic domain wall DW separates the classical orders highlighted as *II* and *III*; the S-0-L distortion pattern changes again to L-0-S and the dipolar $\Uparrow\Uparrow\Downarrow$ pattern is shifted by one site but the magnetic $\uparrow\uparrow\downarrow$ order remains the same at both sides of the domain wall. Dotted lines are added to make apparent the mirror symmetry of the excitation configurations.

magnetic order, all of the six possible (degenerate) magneto-electro-elastic classical plateau configurations are realized along the system length.

We have drawn a schematic description of these results in Fig. 8: the transition between the classical ↑↑↓ plateau regions marked as *I* and *II* is given by a magnetic soliton *MS* passing through a spin singlet, while that between the classical plateau regions *II* and *III* is given by an electroelastic excitation without disruption of the ↑↑↓ magnetic order.

It is interesting to recall an argument based on the bosonized description of the $M = 1/3$ plateau in spin $S = 1/2$ chains, discussed in Ref. [23]. Along this argument, the occurrence of the classical or quantum plateau are related to the vacuum expectation value of a compactified bosonic field. This explains why a soliton interpolating classical configurations must pass over a quantum ordered region as found in that reference and also here in case 2. Conversely, the same argument suggests that a soliton interpolating quantum configurations must pass over a classical order.

In comparing the location of dipolar domain walls ⇓⇑⇑⇑⇓ with respect to the magnetic order, one can extract as a thumb rule that they fit better in the elastic distortions of a classical ↓↑↑↑↓ magnetic environment (see cartoons in Figs. 6 and 8, second line). Thus, when exciting a classical plateau state the dipolar domain walls are located in the classical plateau regions, away from magnetic excitations. Instead, when exciting a quantum plateau state, the dipolar domain walls are located in the classical core of the magnetic solitons, forming a composite MEE quasiparticle.

V. SUMMARY AND CONCLUSIONS

We have explored the interplay between frustrated magnetic and dipolar orders in a one-dimensional model for collinear, type-II multiferroic materials, where electric and magnetic degrees of freedom are indirectly coupled by the lattice distortions. More precisely, we have investigated the commensurability of the $P = 1/3$ period-three dipolar order ⇑⇑⇓ with the period-three magnetic configurations observed in many frustrated magnetic materials within $M = 1/3$ magnetization plateaus.

Both from qualitative arguments and extensive DMRG computations, we have found that the dipolar order introduced by frustrating dipolar interactions competes with the magnetic order set, in turn, by the magnetic frustration at the $M=1/3$ plateau. This opens a nontrivial scenario which we dub *double frustration*. Our analysis provides clear and surprising effects due to this double frustration. In a regime of low anisotropy and high magnetic frustration, favoring quantum fluctuations, the double frustration is responsible for the stabilization of a *quantum $M = 1/3$ plateau* state. In contrast, in all other cases (either introducing higher easy-axis anisotropy and/or reducing magnetic frustration), the second frustration competition leads to the spontaneous parity symmetry breaking in the order of the *classical $M = 1/3$ plateau* state. From this parity breaking mechanism, and in the presence of charge order along the chain, a longitudinal component of the polarization should appear [2]. Detection of different directions of the polarization could be the clue to identify the underlying magnetoelectric effects operating in a given material.

We have also discussed the excitations caused by the increase of the magnetic field. We have found that the $\Delta S^z = 1$ magnon on top of the $M = 1/3$ state fractionalizes into three $S^z = 1/3$ spatially separated solitons, encompassing elastic distortions adapted to the magnetic order. This change in the distortion pattern induces, in the dipolar sector, a spontaneous unit polarization change which, in turn, fractionalizes into three sharp domain walls. Moreover, on top of the quantum plateau state these fractional excitations form a composite magneto-electro-elastic quasiparticle. This emergent magnetoelectric effect, that is, the polarization change induced by a magnetic field mediated by elastic distortions, is an important result in the present paper.

The nature of the plateau-state structure and the appearance of intertwined magnetic and electric fractional excitations, mediated by the lattice, may be experimentally accessible by neutron scattering for the spin channel and by x-ray scattering for the lattice distortions. A candidate material to be explored might be the cobaltite α-CoV$_2$O$_6$, where a $M = 1/3$ magnetization plateau together with strong coupling between magnetic and dielectric order parameters has been reported [20,21]. The striking differences between the present results and those for pure magnetoelastic chains are clear signals of the role of dipolar interactions in multiferroic systems and may guide the search for materials realizing strong magnetoelectric effects.

[1] S.-W. Cheong and M. Mostovoy, Nat. Mater. **6**, 13 (2007).

[2] J. van den Brink and D. I. Khomskii, J. Phys.: Condens. Matter **20**, 434217 (2008).

[3] D. Khomskii, Physics **2**, 20 (2009).

[4] M. L. Medarde, J. Phys.: Condens. Matter **9**, 1679 (1997).

[5] Y. J. Choi, H.-T. Yi, S. Lee, Q. Huang, V. Kiryukhin, and S.-W. Cheong, Phys. Rev. Lett. **100**, 047601 (2008); R. Flint, H.-T. Yi, P. Chandra, S.-W. Cheong, and V. Kiryukhin, Phys. Rev. B **81**, 092402 (2010).

[6] F. Damay, C. Martin, V. Hardy, G. André, S. Petit, and A. Maignan, Phys. Rev. B **83**, 184413 (2011); S. V. Streltsov,

A. I. Poteryaev, and A. N. Rubtsov, J. Phys.: Condens. Matter **27**, 165601 (2015).

[7] I. A. Sergienko, C. Şen, and E. Dagotto, Phys. Rev. Lett. **97**, 227204 (2006).

[8] S. Dong, R. Yu, S. Yunoki, J.-M. Liu, and E. Dagotto, Eur. Phys. J. B **71**, 339 (2009).

[9] Y. Tokunaga, N. Furukawa, H. Sakai, Y. Taguchi, T. Arima, and Y. Tokura, Nat. Mater. **8**, 558 (2009).

[10] G. Giovannetti, A. Stroppa, S. Picozzi, D. Baldomir, V. Pardo, S. Blanco-Canosa, F. Rivadulla, S. Jodlauk, D. Niermann, J. Rohrkamp, T. Lorenz, S. Streltsov, D. I. Khomskii,

and J. Hemberger, Phys. Rev. B **83**, 060402(R) (2011).

[11] S. Catalano, M. Gibert, J. Fowlie, J. Íñiguez, J.-M. Triscone, and J. Kreisel, Rep. Prog. Phys. **81**, 046501 (2018).

[12] J. Blasco, J. L. García-Muñoz, J. García, G. Subías, J. Stankiewicz, J. A. Rodríguez-Velamazán, and C. Ritter, Phys. Rev. B **96**, 024409 (2017).

[13] S. Yáñez-Vilar, E. D. Mun, V. S. Zapf, B. G. Ueland, J. S. Gardner, J. D. Thompson, J. Singleton, M. Sánchez-Andújar, J. Mira, N. Biskup, M. A. Señarís-Rodríguez, and C. D. Batista, Phys. Rev. B **84**, 134427 (2011).

[14] M. K. Kim, J. Y. Moon, S. H. Oh, D. G. Oh, Y. J. Choi, and N. Lee, Sci. Rep. **9**, 5456 (2019).

[15] D. C. Cabra, A. O. Dobry, C. J. Gazza, and G. L. Rossini, Phys. Rev. B **103**, 144421 (2021).

[16] D. C. Cabra, A. O. Dobry, C. J. Gazza, and G. L. Rossini, Phys. Rev. B **100**, 161111(R) (2019).

[17] We use double arrows ⇑, ⇓ in text and graphics to depict dipole orientations, and single arrows ↑, ↓ to depict spin orientations.

[18] K. Okunishi and T. Tonegawa, J. Phys. Soc. Jpn. **72**, 479 (2003).

[19] K. Hida and I. Affleck, J. Phys. Soc. Jpn. **74**, 1849 (2005).

[20] K. Singh, A. Maignan, D. Pelloquin, O. Perez, and Ch. Simon, J. Mater. Chem. **22**, 6436 (2012).

[21] F. Wallington, A. M. Arevalo-Lopez, J. W. Taylor, J. R. Stewart, V. Garcia-Sakai, J. P. Attfield, and C. Stock, Phys. Rev. B **92**, 125116 (2015).

[22] T. Vekua, D. C. Cabra, A. O. Dobry, C. J. Gazza, and D. Poilblanc, Phys. Rev. Lett. **96**, 117205 (2006).

[23] C. J. Gazza, A. O. Dobry, D. C. Cabra, and T. Vekua, Phys. Rev. B **75**, 165104 (2007).

[24] H. D. Rosales and G. L. Rossini, Phys. Rev. B **76**, 224404 (2007).

[25] F. Jin, L. Wang, A. Zhang, J. Ji, Y. Shi, X. Wang, R. Yu, J. Zhang, E. W. Plummer, and Q. Zhang, PNAS **116**, 20322 (2019).

[26] A. E. Feiguin, J. A. Riera, A. O. Dobry, and H. A. Ceccatto, Phys. Rev. B **56**, 14607 (1997).

[27] S. R. White, Phys. Rev. Lett. **69**, 2863 (1992).

[28] K. Okunishi and T. Tonegawa, Phys. Rev. B **68**, 224422 (2003).

[29] M. Fishman, S. R. White, and E. Miles Stoudenmire, arXiv:2007.14822.

[30] See Supplemental Material at http://link.aps.org/supplemental/10.1103/PhysRevB.105.115103 for numerical results at $\Delta = 1$, $J_2/J_1 = 0.8$, and $\Delta = 4$, $J_2/J_1 = 0.5$.

[31] T. Nakano and H. Fukuyama, J. Phys. Soc. Jpn. **49**, 1679 (1980).

[32] L. D. Fadeev and L. Takhtajan, Phys. Lett. A **85**, 375 (1981).

[33] V. Kiryukhin, B. Keimer, J. P. Hill, and A. Vigliante, Phys. Rev. Lett. **76**, 4608 (1996).

[34] A. Dobry and D. Ibaceta, Phys. Rev. B **63**, 144404 (2001).

[35] T. Lorenz, B. Büchner, P. H. M. van Loosdrecht, F. Schönfeld, G. Chouteau, A. Revcolevschi, and G. Dhalenne, Phys. Rev. Lett. **81**, 148 (1998).

[36] M. Horvatić, Y. Fagot-Revurat, C. Berthier, G. Dhalenne, and A. Revcolevschi, Phys. Rev. Lett. **83**, 420 (1999).